An analytical model to predict the depth of sub-surface damage for grinding of brittle materials

Jingfei Yin[1], Qian Bai[2], Saurav Goel[3,4,5,6], Ping Zhou[2] and Bi Zhang[7*]

[1] College of Mechanical and Electrical Engineering, Nanjing University of Aeronautics and Astronautics, Nanjing 210016, China
[2] School of Mechanical Engineering, Dalian University of Technology, Dalian 116024, China
[3] School of Engineering, London South Bank University, 103 Borough Road, London SE1 0AA, UK
[4] School of Aerospace, Transport and Manufacturing, Cranfield University, Bedfordshire, MK43 0AL, UK
[5] Department of Mechanical Engineering, Shiv Nadar University, Gautam Budh Nagar, 201314, India
[6] EPSRC Centre for Doctoral Training in Ultra-Precision Engineering, University of Cambridge and Cranfield University, UK
[7] Department of Mechanical and Energy Engineering, Southern University of Science and Technology, Shenzhen 518055, China

*Corresponding author: zhangb@sustech.edu.cn

Abstract: This paper proposes an analytical model for predicting grinding-induced sub-surface damage depth in a silicon wafer. The model integrates the dislocation kinetics for crack initiation and fracture mechanics for crack propagation for the first time. Unlike other conventional models, the proposed model considers the effects of strain rate on damage depth and the dynamically changing metastable phase change properties. The model is verified by grinding experiments and a comparison of theoretical and experimental results shows a good quantitative agreement. It is found that increasing grinding speed and decreasing depth of cut cause a higher strain rate so as to enhance material brittleness, which is favorable to achieving low sub-surface damage. These findings will pave a way towards optimizing the grinding parameters and greatly improving the production efficiency of hard and brittle materials.

Keywords: silicon; analytical model; sub-surface damage; dislocation; fracture mechanics

Abbreviations:

DOC	*Depth of cut*
FEM	*Finite element method*
L-C	Lomer-Cottrell lock type of dislocations
SSD	*Sub-surface damage*
MD	*Molecular dynamics*
HPPT	*High pressure phase transformation*
BK7	A grade of *Borosilikatglas from Schott Glaswerke AG*

Nomenclature

δ	Subsurface damage depth
F, F_N	Average machining force, normal machining force
p_n, α, β, ζ, χ, ψ, η, κ, p, q, m, n, $\dot{\varepsilon}_0$	Constants
a_c	Depth of cut
E, E_i, E_e	Elastic module of the workpiece, elastic modulus of the cutting tool, effective modulus
v, v_i	Poisson's ratio of the workpiece, Poisson's ratio of the cutting tool
k	Boltzmann constant
T	Temperature
K_C, K_{Cd}	Static fracture toughness, dynamic fracture toughness
H, H_d	Static hardness, dynamic hardness
R	Radius of the abrasive grain
r	Radial distance from the center of the wafer
R_s	Radius of the grinding wheel
c	Crack size
σ_{fl}, σ_F	Flow stress, fracture stress
ΔG	Activation free energy
F_0	Total free energy
$\bar{M}$	Taylor factor
$\hat{\tau}$	Maximum glide resistance
ρ_m	Mobile dislocation density
b	Burger's vector
B	Drag coefficient of dislocation
v	Dislocation speed
V	Surface speed of the grinding wheel

$\dot{\varepsilon}$	Strain rate
f	Feed rate of the grinding wheel
γ	Concentration of the grinding wheel
W	Width of the abrasive segment of the grinding wheel
L	Total length of abrasive segments
N_w, N_s	Rotational speed of the workpiece, rotation speed of the grinding wheel

1. Introduction

Due to its abundance and excellent electronic properties, silicon dominated the semiconductor consumer market for much of the 20th century. Silicon is the most studied semiconductor material in recent decades, and a modicum of success has been achieved, making it a relatively well understood material compared to the others [1]. This is the primary reason that silicon will continue to play a significant role in the advanced and miniaturized products in the electronics and optics sector.

The relatively low fracture toughness of silicon of about 0.9 MPa m$^{1/2}$ makes it a hard, brittle, and difficult-to-cut material [2]. Surface integrity is often discussed in terms of the state of the machined surface and sub-surface, and the term is used to describe attributes such as sub-surface damage (SSD), high-pressure phase transformation, cracking, brittle fracture, residual stress, microstructural twinning, which are useful in assessing the quality of a machined part. SSD is detrimental to the service performance, especially the fatigue life, of the machined part.

It has, therefore, remained at the heart of machining research endeavors to predict sub-surface damage depth in silicon subjected to cutting or grinding [3-6]. Most researches are based on the damage model proposed by Lawn and Wilshaw [7] for brittle materials, resulting in the researches focusing on the subsurface crack system. However, few studies take into considerations the stage before crack initiation to predict the depth of SSD. It is the motivation of this study to explore what takes place before the crack initiation and to reveal the contribution of the stage before the crack initiation to the distribution of SSD in a ground silicon wafer.

Researchers have been attempting to establish a relationship between SSD and process parameters. For example, Sun et al. [6] developed a grinding force model to predict SSD depth. In this model, grinding forces were assumed to be solely dependent on the depth of cut (DOC) of abrasive grains. SSD depth was found to be linearly proportional to the grinding force with a power index of 2/3, in line with other research studies [8-10]. Malkin and Hwang [11] came up with clarification and suggested that the power index should depend on loading conditions, especially in machining of

ceramics. Zhang and Howes [12] studied grinding-induced SSD of ceramics and found that the SSD depth follows a power law of DOC and that the power index can be determined by the hardness and fracture toughness of the workpiece material.

These studies have three key limitations, which in fact, provides a new ground for us to undertake this study to overcome the limitations:

(i) These studies are based on classical fracture mechanics which was drawn from the Griffith theory by assuming pre-existing defects to initiate and propagate a crack in the material [13]. However, the modern manufacturing technology allows fabrication of the monocrystalline silicon without any macroscopic defects or cracks. Hence, the Griffith theory cannot be applied to handling crack initiation problems in a nearly perfect material.

(ii) The second limitation is that they are primarily based on depth of cut (DOC) considerations while other parameters, e.g., wheel speed and feed rate, can also affect the SSD depth. As this paper shows, besides DOC, cutting speed is also an influential parameter as it directly dictates the applied strain rate. An increase in the cutting speed reduces SSD. Gao et al. [14, 15] studied SSD of monocrystalline silicon from a wire-sawing process and found that a higher wire speed reduced the SSD. Wang et al. [16] used FEM simulations and studied SSD in grinding of BK7. He also performed experiments at a grinding speed ranging from 60-120 m/s. Their results showed a good surface finish and reduced SSD depth at higher cutting speeds. Similar conclusions were reached during grinding of other hard and brittle materials, such as Si_3N_4 [17, 18], fused silica [19], and SiC [20].

(iii) The third limitation is that they used static material properties acquired from the standard static/quasi-static testing at an infinitesimal strain rate, typically lower than 1 s^{-1}. However, in the practical machining processes, strain rate is considerably high, ranging from 10^3 to 10^6 s^{-1}, or even higher. Since material properties are strain-rate sensitive [21], errors would be induced if the static properties were used to predict SSD depth in a dynamic machining process at a high strain rate.

Goel et al. [22] recently showed how the strain rate at the nanoscale made a remarkable difference in influencing the mechanical properties of the monocrystalline silicon. It is noteworthy that depending on the length scale, the process of ductile mode cutting of silicon entails the occurrence of high-pressure phase transformation and such events bring about few metastable and stable phases of silicon. Depending on the stress state (or strain rate applied), such phases can be amorphous or crystalline and their mechanical properties are different from the pristine silicon [23]. Hitherto, these events have never been considered in the existing models.

Wu et al. [21] claimed that the failure strength and fracture toughness increased with strain rate during high-speed machining. Liu et al. [20] proposed that during high-speed grinding of SiC, the dynamic fracture toughness was proportional to the logarithm of strain rate. Limbach et al. [24] investigated the strain-rate sensitivity of the localized plastic

deformation in glass and reported that the glass having Poisson's ratio of 0.3-0.4 showed high strain-rate dependency. Chaudhri et al. [25] from their nano impact experiments noticed that the dynamic hardness increases with strain rate. Overall, the material property evolves with the cutting process and changes dynamically.

The limitations of the existing models are highlighted in Table 1.

Table 1. Limitations of the current prediction models

Predictive models	Limitations
$\delta = p_1 \cdot F^{2/3}$ [6-9]	1. Based on the Griffith's assumption this model just considered crack propagation, without considering crack initiation. 2. It used the static material properties and neglected the strain rate effects. 3. As a first attempt, it was a simplified model which considered only the depth of cut as key input and neglected other process parameters.
$\delta = p_2 \cdot F^n,\ n = 2/3$ or 8/9 [10]	
$\delta = p_3 \cdot a_c^{1/\log(H/K_c)}$ [11]	The model used the static material properties and neglected the strain rate effects on material properties.

In predicting SSD depth in a silicon wafer, Li et al. [5] identified that elastic modulus and fracture toughness degraded with an increase in grinding speed. Wu et al. [21] reported that an increase in grinding speed diminishes grinding damage in SiC. However, very few studies are based on the fundamental mechanisms of material property changes. The changes in the macroscopic properties of a material turn out to be a result of the mismatch and distortion of lattice structures, i.e., dislocations. In plastic materials, crack initiation is generally caused by the accumulation and burst of dislocation pile-up [26]. In the monocrystalline silicon wafer, crack initiation was suggested to attribute to the Lomer-Cottrell (L-C) locks from dislocation intersections [27]. Bulatov et al. [28] reported the formation of Lomer-Cottrell locks in cracking the FCC metals based on molecular dynamics. They found two dislocations kinked to form an L-C lock which obstructed the dislocation motion. Chavoshi et al. [29] studied plasticity of the monocrystalline silicon in the nanometric cutting with the MD simulation. The simulation result revealed that along with the amorphization and dislocations, stacking faults were also generate in the (110) [001] cutting, which would increase the possibility of the dislocation interaction and the formation of the L-C locks.

Chavoshi et al. [30] also simulated cutting of 3C–SiC along the $(110)\ \langle 00\bar{1} \rangle$ orientation under various temperature conditions. They observed the formation and

destruction of the stacking fault-couple bounding between the partial dislocation segments and L-C locks. Once a crack is initiated, its propagation can be estimated by using the theory of fracture mechanics.

The main motivation of this paper is to advance the current understanding of this topic by incorporating strain rate effect with the crack propagation theory during grinding of monocrystalline silicon. The paper uses the dislocation kinetics theory for crack initiation and fracture mechanics theory of crack propagation to improve the prediction accuracy of SSD depth during grinding.

One must understand here that generally, there are two kinds of subsurface cracks observed during machining of monocrystalline silicon, namely, microcracks filled with phase-transformed silicon [31], and open cracks which propagate deep into the bulk material [32]. The paper deals with the open cracks as the understanding of the former is still in infancy. Also, the opened cracks are assumed to initiate from the L-C locks and the junctions of dislocations. Besides cracks and dislocations, phase transformation happens in machining, which is caused by high pressure phase transformation (HPPT) [1]. HPPT area generally forms just close to the cutting edge. There was hardly reported that HPPT had any relations with the subsurface cracks. Therefore, the paper focuses on the subsurface cracks neglecting the influence of phase transformation.

2. Physical model for SSD depth prediction

In numerous studies, SSD depth, δ, has been correlated with normal force or thrust force, F_N [6, 8-11, 17] as below

$$\delta \propto {F_N}^n \tag{1}$$

where n depends on the cutting conditions and the geometry of a cutting tool. Based on the Hertzian contact theory, the normal force exerted by an abrasive grain in grinding can be estimated from Eq. (2) [6, 33]

$$F_N = \frac{4}{3} \cdot E_e \sqrt{R} {a_c}^{3/2} \tag{2}$$

where E_e is the effective modulus which is related to Young's modulus and Poisson's ratio of the workpiece and the abrasive grain. R and a_c are the radius of the abrasive grain and depth of cut (DOC), respectively. The effective modulus can be resolved as below [33].

$$\frac{1}{E_e} = \frac{1-\nu^2}{E} + \frac{1-{\nu_i}^2}{E_i} \tag{3}$$

where E, ν, E_i, and ν_i are the elastic modulus and Poisson's ratio of the workpiece and the single grit of the abrasive grains, respectively. Therefore, combining Eqs. (1) and (2)

$$\delta \propto a_c^{\chi} \tag{4}$$

such that χ is an exponent dependent on the ratio of hardness and fracture toughness H/K_C of the substrate [12]. In Ref. [12], Zhang and Howes demonstrated that the exponent χ follows the inverse of the log of H/K_C in grinding of hard and brittle materials. However, they used the static material properties. Since this study considers the effects of strain rate on the material properties, the material dynamic properties are used, as shown by Eq. (5)

$$\delta \propto a_c^{1/\log(H_d/K_{Cd})} \tag{5}$$

where H_d and K_{Cd} are the dynamic hardness and dynamic fracture toughness of the monocrystalline silicon. The ratio of the dynamic hardness and the dynamic fracture toughness represents the dynamic brittleness of the material.

A general analytical model presented in this paper is shown in Fig. 1. At the microscopic level, dislocations are initiated and activated by an external load and greatly affected by the strain rate in a loading process [34]. The interactions among the dislocations, including entanglement and immobilization forming L-C locks, lead to crack initiation.

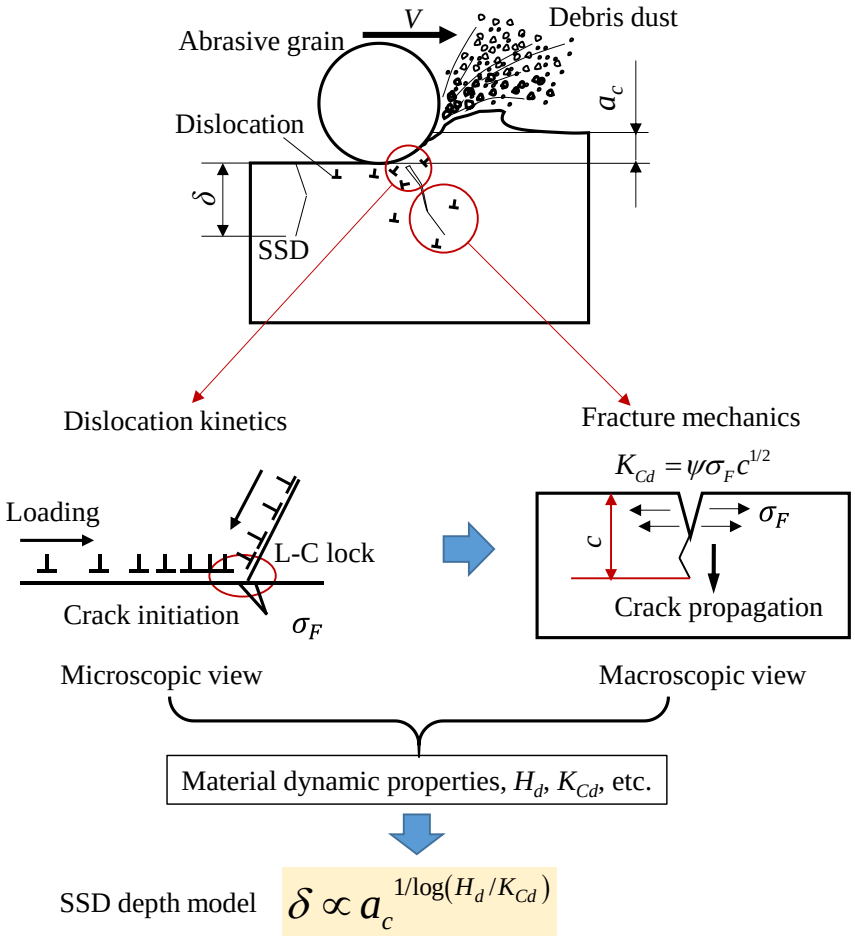

Fig. 1: General illustration of the analytical model developed in this study

Once a crack is initiated, its propagation can be analyzed by fracture mechanics at the macroscopic level. Therefore, the dynamic properties can be analyzed in terms of strain-rate sensitivity by incorporating the dislocation kinetics and fracture mechanics. Finally, the dependency of the SSD depth on the process parameters and material dynamic properties can be established and predicted.

Previous investigations demonstrated that the dynamic hardness of a material is proportional to its flow stress [35] and is expressed by Eq. (6)

$$H_d = \alpha \cdot \sigma_{fl} \tag{6}$$

where σ_{fl} is the flow stress of the material; α is a constant determined by the ratio of elastic modulus E to yield strength Y [35-37]. For a monocrystalline silicon wafer, α was calculated as 3 [38].

It should also be noted that both hardness and fracture toughness change strain rate [34]. Dynamic fracture toughness K_{Cd} can be estimated by Eq. (7) [11, 39]

$$K_{Cd} = \beta \cdot \left(\frac{E}{H_d}\right)^{1/2} \left(\frac{F_N}{c^{3/2}}\right) \tag{7}$$

where c is the crack size; β is a constant related to the geometry of an abrasive.
Based on the fracture mechanics, fracture toughness can be estimated by Eq. (8) as [40]

$$K_{Cd} = \psi \sigma_F c^{1/2} \tag{8}$$

where ψ and σ_F are the dimensionless geometric term and fracture stress, respectively. For the monocrystalline silicon, fracture stress, σ_F is assumed to be equal to flow stress, σ_{fl} at room temperature [41]. Therefore, substituting Eq. (8) into Eq. (7) leads to the dynamic fracture toughness expressed in Eq. (9) as

$$K_{Cd} = \zeta \left[\left(\frac{E}{H_d}\right)^{1/2} \cdot F_N \sigma_{fl}^{\ 3} \right]^{1/4} \tag{9}$$

where $\zeta = \beta^{1/4}\psi^{3/4}$, it is a constant determined by the geometry of the cutting edge. Eq. (9) no longer uses crack size c for fracture toughness. The dynamic fracture toughness K_{Cd} can be obtained in terms of flow stress.

Therefore, the predictive model can be derived as Eq. (10).

$$\delta = \kappa \cdot a_c^{1 \Big/ \log\left[\frac{\eta}{\sqrt{ER}}\left(\frac{1-\nu^2}{E}+\frac{1-\nu_i^2}{E_i}\right)\left(\frac{\sigma_{fl}}{a_c}\right)^{3/2}\right]^{1/4}} \tag{10}$$

where κ, η are the dimensionless constants determined by the geometry of the cutting edge, workpiece material properties, and loading conditions.

The flow stress is related to the motion of dislocations in a material. The motion of

dislocations is controlled by two mechanisms, i.e., the thermal activation at low strain rates and the dislocation drag at high strain rates, depending on the strain rates. Based on the pure thermal activation, the general relationship is given in Eq. (11) [42] as

$$\dot{\varepsilon} = \dot{\varepsilon}_0 \exp(-\Delta G / kT) \tag{11}$$

where $\dot{\varepsilon}_0$ is a microstructural dependent pre-exponential constant and is used for calculating the strain rate under given applied stress and temperature conditions; ΔG, k, and T are the activation free energy, Boltzmann constant, and temperature, respectively. The activation free energy ΔG can be described by Eq. (12) [43]

$$\Delta G = F_0[1-(\sigma_f / (\bar{M}\hat{\tau}))^p]^q \tag{12}$$

where F_0 is the total free energy; $\bar{M}$ is the appropriate Taylor factor; $\hat{\tau}$ is the maximum glide resistance, and exponents p and q describe the obstacle profile. The flow stress can be resolved by rearranging Eq. (13) as

$$\sigma_f = \left(\bar{M}\hat{\tau}\right)\cdot\left[1+\frac{kT}{F_0}\left(\ln\dot{\varepsilon}-\ln\dot{\varepsilon}_0\right)\right]^{1/(pq)} \tag{13}$$

For single- and polycrystalline metals, the set p=1/2 and q=3/2 are the most commonly used [42]. If p=q=1 is considered, then it represents a rectangular obstacle and a regular lattice arrangement to the obstacle. For the monocrystalline silicon, p=q=1 can be considered. Therefore, the flow stress can be calculated by Eq. (14) as

$$\sigma_{fl} = \left(\bar{M}\hat{\tau}\right)\cdot\left[1+\frac{kT}{F_0}\left(\ln\dot{\varepsilon}-\ln\dot{\varepsilon}_0\right)\right] \tag{14}$$

As strain rate increases, the dominant mechanism controlling the dislocation motion gradually transits from thermal activation to dislocation drag. If dislocation velocity is purely controlled by the lattice drag, a relationship can be expressed as [42]

$$v = \sigma_{fl} b / \bar{M}B \tag{15}$$

where b and B are Burger's vector and drag coefficient, respectively. According to Orowan's equation [44] of rheology

$$\dot{\varepsilon} / \bar{M} = \rho_m b v \tag{16}$$

where ρ_m refers to the mobile dislocation density.

Therefore, by combining Eqs. (15) and (16), the dislocation velocity v can be eliminated and the flow stress in the dislocation drag regime can be calculated from Eq. (17)

$$\sigma_{fl} = \frac{B}{\rho_m b^2}\dot{\varepsilon} \tag{17}$$

However, the mobile dislocation density ρ_m is not a constant, but sensitive to the applied

stress and strain rate. The variation in the mobile dislocation density as a function of the applied stress is still an open question. Regazzoni et al. [42] provided a framework to describe the behaviour of the mobile dislocation density, as shown in Eq. (18)

$$\rho_m \propto \left(\frac{\sigma_{fl}}{\bar{M}\hat{\tau}} \right)^{\eta} \tag{18}$$

Substituting Eq. (18) into Eq. (17), it can be found that flow stress is dependent on strain rate with a power index smaller than one.

Zaretsky and Kanel [45] proposed an explicit relationship between mobile dislocation density and strain rate to express the flow stress of an aluminum alloy under shock loading, as given by Eq. (19)

$$\rho_m \propto \dot{\varepsilon}^{2/3} \tag{19}$$

Substituting Eq. (19) into Eq. (17) shows that the flow stress is dependent on strain rate with a power index of 1/3. The previous experimental results demonstrated that the flow stress increased at high strain rates. $\sigma_{fl} \propto \dot{\varepsilon}^{0.25}$ for some metals and brittle materials [46-48], while $\sigma_{fl} \propto \dot{\varepsilon}^{1/3}$ for rocks [49], although these materials have a commonality in low power indices of strain rate.

For simplification, the dependence of the flow stress on strain rate at higher strain rates (such as during grinding) for a monocrystalline silicon wafer can be expressed by Eq. (20) as

$$\sigma_{fl} \propto \dot{\varepsilon}^{m} \tag{20}$$

where $m \leq 1/3$.

Wang et al. [50] suggest that the strain rate in grinding be correlated with the grinding speed and DOC as Eq. (21)

$$\dot{\varepsilon} = V / a_c \tag{21}$$

Generally, the maximum DOC dominates the grinding-induced SSD. A schematic diagram of the relative motion of the silicon wafer with respect to the grinding wheel is shown in Fig. 2. The density of the grinding marks near the center of the wafer is larger than that close to the periphery. However, material removal rate is considered uniform along the radial direction of the wafer. Based on the geometric rotational trajectories of the abrasive grains, neglecting the elastic deformation of the grinding system, the maximum DOC during self-rotating grinding can be calculated by using Eq. (22) [6]

$$a_c = 4.88 \cdot R \left[\frac{rfN_w}{LW\gamma N_s^2 \left(1 + \frac{r^2}{8R_s^2} \right)} \right]^{0.4} \tag{22}$$

where r is the radial distance from the center of the wafer; R_s is the radius of the grinding wheel; L is the total segment length; W is segment width; γ is the volume concentration of the grinding wheel; N_w, N_s, and f are worktable speed, wheel speed, and feed rate, respectively.

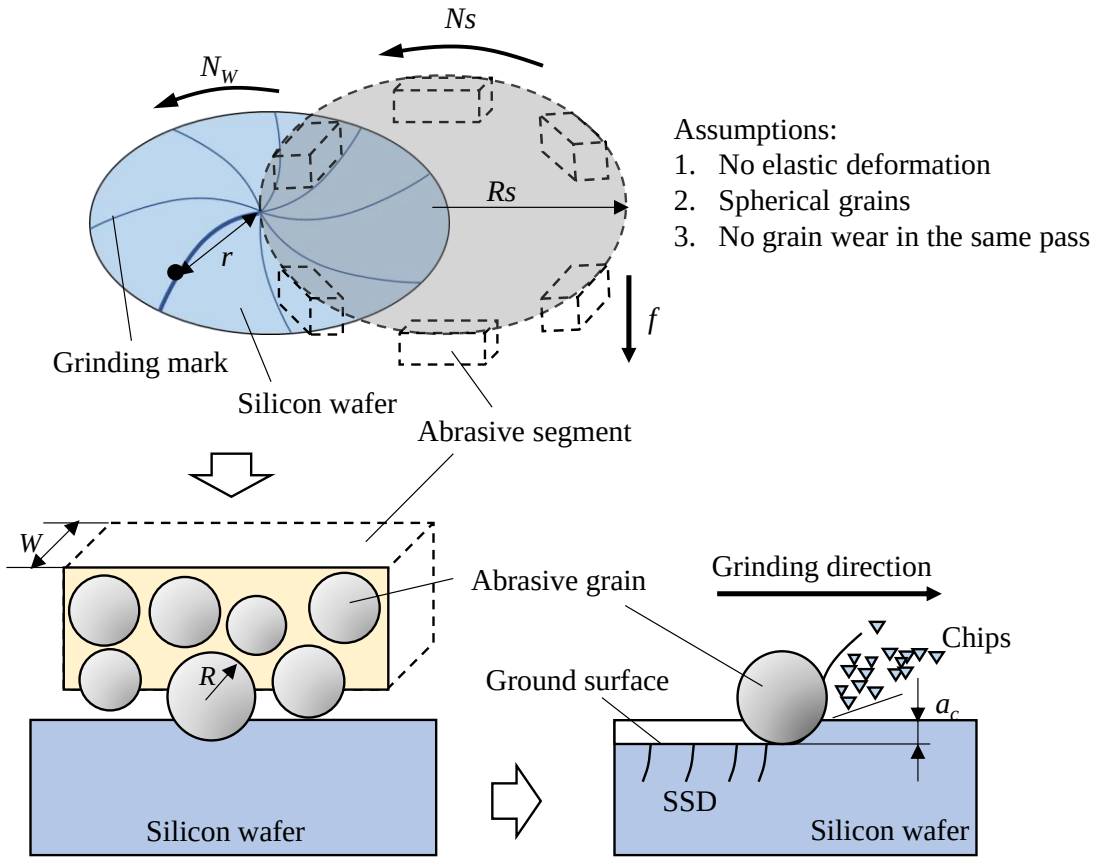

Fig. 2: Schematic diagram of the relative motions between grinding wheel and wafer

Therefore, the flow stress is calculated based on Eq. (23)

$$\begin{cases} \sigma_{fl} = f_1(T) \cdot ln(V_C/a_c) + f_2(T) & \text{at high strain rates} \\ \sigma_{fl} \propto (V_C/a_c)^m & \text{at low strain rates} \end{cases} \tag{23}$$

where $f_1(T)$ and $f_2(T)$ are temperature-related coefficients. During the self-rotating grinding of a silicon wafer, temperature rise can be suppressed by sufficient coolant supply. Therefore, the effect of temperature rise was neglected in this paper.

Smith et al. [51] studied the dynamic responses of silicon to the shock loading with a wide range of strain rates from 10^5 to 10^9 s^{-1}. They found that the critical transition strain rate is 10^7 s^{-1} below which dislocation movement is dominated by thermal activation whereas a strain rate higher than 10^7 s^{-1} makes dislocation drag to dominate the dislocation movement. Therefore, this paper adopts the fitting equations proposed by Smith et al. to describe the variation of flow stress with strain rate, as shown in Eq. (24)

$$\begin{cases} \sigma_{fl} = 4.06 + 0.32 \ln \dot{\varepsilon} & \dot{\varepsilon} \le 10^7 \ s^{-1} \\ \sigma_{fl} = 0.32 \dot{\varepsilon}^{0.21 \pm 0.02} & \dot{\varepsilon} > 10^7 \ s^{-1} \end{cases} \tag{24}$$

The flow stresses in Eq. (24) at different strain rates are used to arrive at a robust SSD prediction model (i.e. Eq. (10)) during self-rotating grinding by considering the flow stress and dynamic properties of the monocrystalline silicon.

3. Experimental study

In the experimental study, monocrystalline silicon wafers were machined by the self-rotating grinding on a high-precision grinding machine (VG401 MKII, Okamoto, Japan). Much like the other machining processes, SSD in silicon during self-rotating grinding is directly related to the process parameters, namely grinding wheel diameter, rotational speed, and feed rate, as shown in Fig 3. A silicon wafer was fixed on the worktable by a vacuum chuck. The grinding wheel was the cup-type with abrasive segments uniformly installed around the periphery of the wheel. In grinding, the wafer rotated with the worktable that had the traces of the abrasive segments passing through the center of the wafer. The grinding wheel moved downward in feeding to thin the wafer.

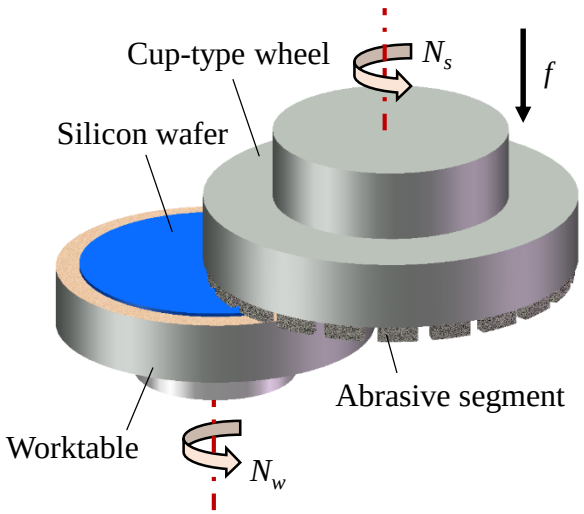

Fig 3: A schematic illustration of self-rotating grinding setup

Grinding parameters are listed in Table 2. The wafers used were with the (100) surface and a diameter of 200 mm. Each wafer was thinned to 50 μm in thickness. Two cup-type diamond wheels of mesh numbers of #600 and #400 were used in grinding to induce two different depths of SSD. The #600 wheel was resin-bonded while the #400 was vitrified-bonded, as shown in Fig. 4. The specifications of the grinding wheels are shown in Table 3.

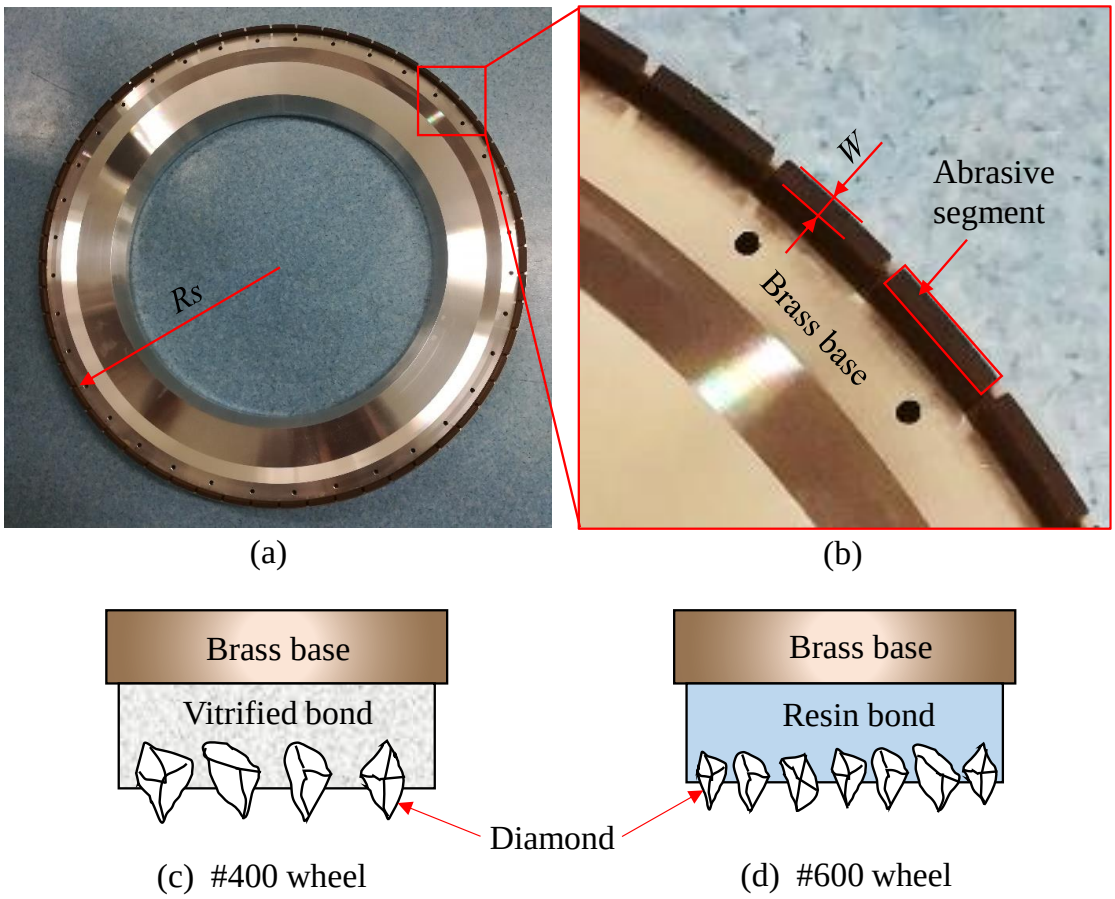

Fig. 4: Photographic views and schematics of the grinding wheels. (a) Photographic view of the grinding wheel, (b) zoom-in view of the inset in (a), (c) schematics of #400 wheel construction, (d) schematics of #600 wheel construction.

Table 2. Grinding parameters for the silicon wafers

Parameters	Values
Wheel speed N_s, r/min	2399
Worktable speed N_w, r/min	120
Feed rate f, μm/min	90
Coolant	Deionized water

Table 3. Specifications of the grinding wheels

Specifications	Values
Wheel diameter, mm	350
Total segment length L, mm	934
Segment width W, mm	3
Wheel concentration/%	100

In the experimental study, both the microstructures and SSD of the ground wafers were examined. The examination of the microstructures could help reveal the physical changes in the wafer material due to grinding and was conducted with a transmission electron microscope (TEM) (Titan Cubed Themis G2 300, FEI, USA). SSD depth was measured by the cross-sectional microscopy and used to verify the proposed model. The details of the sampling and detection methods were reported elsewhere [52]. The radial distribution of SSD was investigated. Four locations at the distances of 20, 40, 60, and 80 mm away from the center of the wafers were chosen for the SSD measurements. The measurement of SSD depth at each location repeated three times.

The depth of SSD induced in grinding was predicted with the proposed physical model. By comparing the predicted SSD depth with the detection values, the proposed model was rationalized. Based on the model, the variation of the material dynamic properties with the process parameters was studied. SSD formation was also analyzed and discussed in the paper in terms of the changes in material properties, including elastic modulus, Poisson's ratio, dynamic hardness and toughness, and the process parameters. Among the process parameters, grinding speed and DOC were the most important in the model. Grinding speed in a range of 10-100 m/s and grain-wise DOC with 0.01-1 μm were used to study the influence of the material property changes on SSD since the ranges have generally been adopted in other studies [6, 52, 53].

Many studies considered elastic modulus and Poisson's ratio as material constants in machining without a reasonable explanation. However, Hayes et al. [54] studied the material properties of copper under the shock loading conditions and found that Poisson's ratio rose from the initial value of 0.356 to 0.5 at the Hugoniot pressure of 2.32 Mbar and shear modulus rose from 44 GPa to 120 GPa and dropped precipitously when the shock caused material melting. The Hugoniot pressure is related to impact speed, i.e., strain rate [55]. During grinding of silicon wafers, strain rate is considerably high. Therefore, it is necessary to investigate the effects of the changes in elastic modulus and Poisson's ratio on the SSD depth in grinding, to our knowledge, which has not been reported before.

4. Results

Figure 5 shows the TEM images of the wafer surface ground with the #600 wheel. The topmost is an amorphous layer marked with α-Si beneath which cracks and dislocations are observed. In Fig. 5 (a), there are stress-induced stripes which disturb the observation of dislocations. Dislocations are visible in the enlarged inset A shown in Fig. 5 (b). As shown in ellipse B in Fig. 5 (b), the dislocations kink each other to form L-C locks which may obstruct further dislocation movements and lead to stress concentration, and finally crack initiation, similar to crack initiation in plastic materials [26].

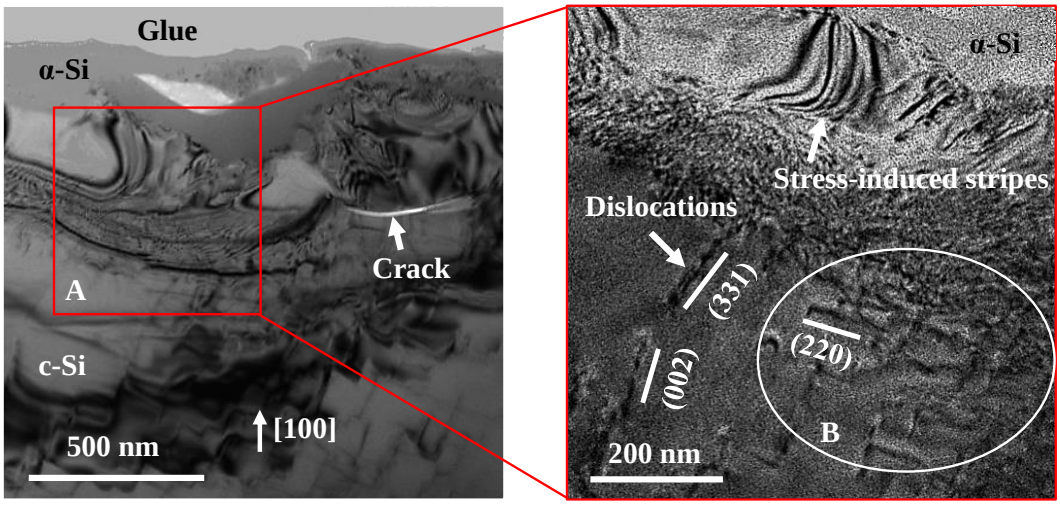

Fig. 5: TEM images of the silicon wafer ground by the #600 wheel. (a) low-power field, (b) the inset of A in (a). α-Si: amorphous silicon, c-Si: crystal silicon.

As shown in Fig. 6, SSD depth in the #400 wheel ground wafer linearly increases with $a_c^{1/\log(H_d/K_{Cd})}$. It shows that the SSD obtained in the experiments by Sun et al. [6] presents in the same tendency. The data points are linearly fitted, and the fitting equation has been used to predict SSD induced by the #600 wheel grinding. Fig. 7 shows the predictions of the SSD depth of the wafers ground by the #600 wheel. The predicted SSD depth increases with the distance away from the wafer center, which is coincident with the situation of the practically detected SSD depth. However, when using the maximum DOC per grain a_c to predict damage depth, the prediction shows a larger error compared to the experimental measurements. The reason for the larger error of the prediction with a_c could be due to the elastic deformation of the grinding system during grinding. In the previous modelling, an assumption was made that there was no elastic deformation in the grinding system. The assumption makes sense in grinding with the #400 wheel of the vitrified bond that provides a high stiffness. However, the #600 wheel was made of the resin bond of which the stiffness is far lower than the vitrified bond. During grinding, the resin bond may be pushed back by the abrasive

grain due to grinding force, which reduces actual DOC per grain and the SSD depth, accordingly. When using the half of the maximum DOC, i.e., $a_c/2$, the prediction errors are within an acceptable range, as shown in Fig. 7. Therefore, it is more reasonable to consider the deformation of the wheel bond in predicting damage depth in the silicon wafer ground with the #600 wheel.

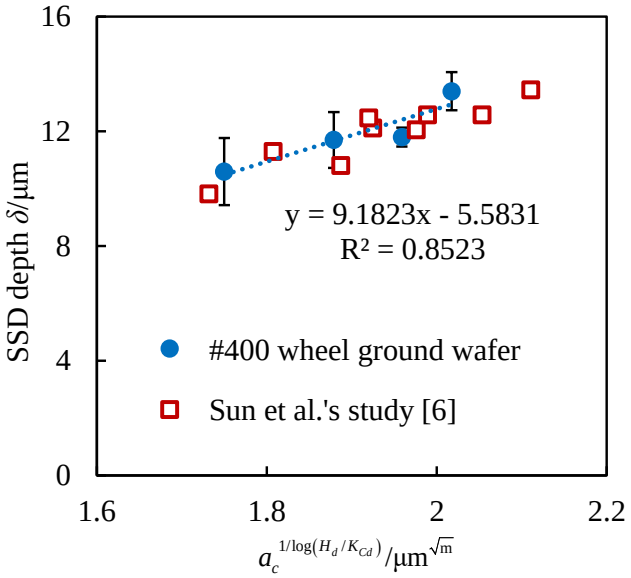

Fig. 6: Relationship between SSD depth δ and $a_c^{1/\log(H_d/K_{Cd})}$

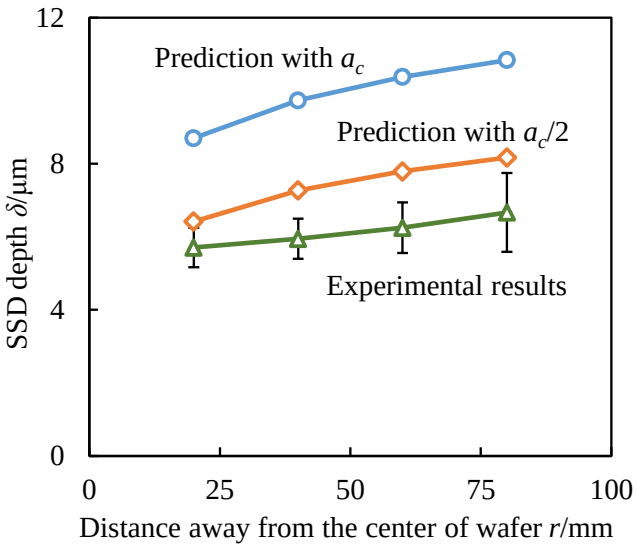

Fig. 7: SSD depth distribution over the wafer ground with the #600 wheel grinding

Figure 8 shows a comparison of the predicted SSD depth by the newly proposed model with the experimental results in Ref. [6] in the different grinding conditions. The model predicts the experimental results with an average error of 4.4%. The variation in SSD depth is opposite to that of the calculated strain rates. SSD depth decreases with an increase in strain rate, and vice versa. It turns out that increasing the strain rate has a positive effect on decreasing SSD depth.

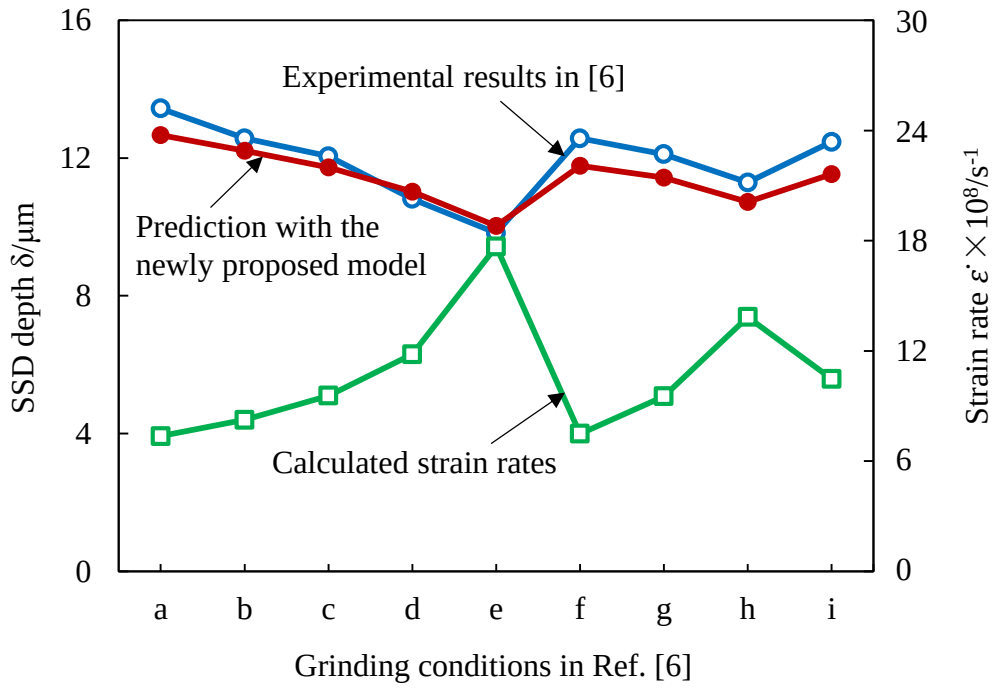

Fig. 8: Comparison of the SSD depth predicted by the newly proposed model with the experimental results in Ref. [6] (Feed rate *f*/(μm/min): a-e were 120, 96, 72, 48, 24, f-i were all 48; wheel speed *Ns*/(r/min): a-e, h and i are 5000, f and g were 4000 and 4500; wafer speed *Nw*/(r/min): a-g were 200, h and i are 150 and 250, respectively.)

In the model, the ratio of dynamic hardness to dynamic fracture toughness H_d/K_{Cd} can be regarded as an index for material dynamic brittleness [38]. Both the dynamic hardness and dynamic fracture toughness are highly strain-rate dependent. Therefore, the dynamic brittleness of silicon in grinding is also dependent on the strain rate. Fig. 9 shows that increasing grinding speed enhances the dynamic brittleness of the silicon wafer, which is due to the elevated strain rate. The strain rate in grinding with the #600 wheel is larger than that in grinding with the #400 wheel under the same processing conditions, so is the dynamic brittleness of the silicon wafer. The difference in the dynamic brittleness in the grinding by the two wheels mainly results from the depth of cut of a single diamond grain. Based on Eq. (22), the #400 wheel has larger diamond grain size than the #600 wheel, which produces larger depth of cut of a single diamond grain. As calculated by Eq. (21), the strain rate in the grinding by the #400 wheel is lower. Correspondingly, the dynamic brittleness in the grinding with the #400 wheel is smaller than with the #600 wheel. As the grinding speed is elevated, the increasing rate of the dynamic brittleness decreases. Fig. 9 also shows that the dynamic brittleness has a limit.

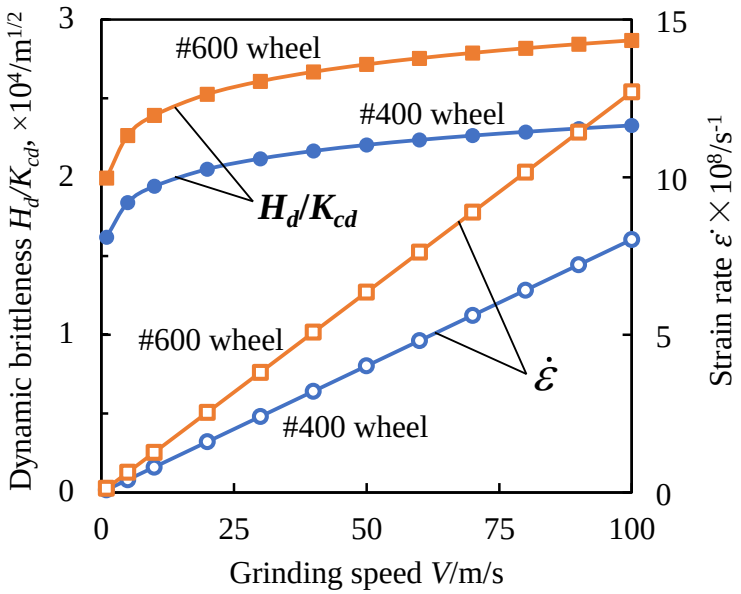

Fig. 9: Variation of the dynamic brittleness H_d/K_{Cd} and strain rate with grinding speed

Figure 10 shows that SSD depth indeed increases with elastic modulus and Poisson's ratio. However, the tendencies to increase are hardly noticeable. The increment in SSD depth is less than 3% over a three-time span of the elastic modulus E'. The increment with Poisson's ratio is even smaller, less 0.2%, with the Poisson's ratio doubled. Therefore, the effects of the material elastic modulus and Poisson's ratio can be neglected in modelling SSD depth. Fig. 10 provides good reasoning for justifying the material elastic modulus and Poisson's ratio which were considered as constants in the previous studies [6, 21].

Furthermore, it suggests that the effects of the anisotropy of monocrystalline silicon wafer on damage depth might be weakening in machining at a high strain rate. In quasi-static testing conditions, monocrystalline silicon presents distinct anisotropy. In the high strain rate grinding, the dynamic material properties, such as elastic modulus, Poisson's ratio, fracture toughness, etc., all change. The changes in the material properties could result from the change in the lattice structure or the arrangement of atoms which may render the material response to the grinding process isotropic.

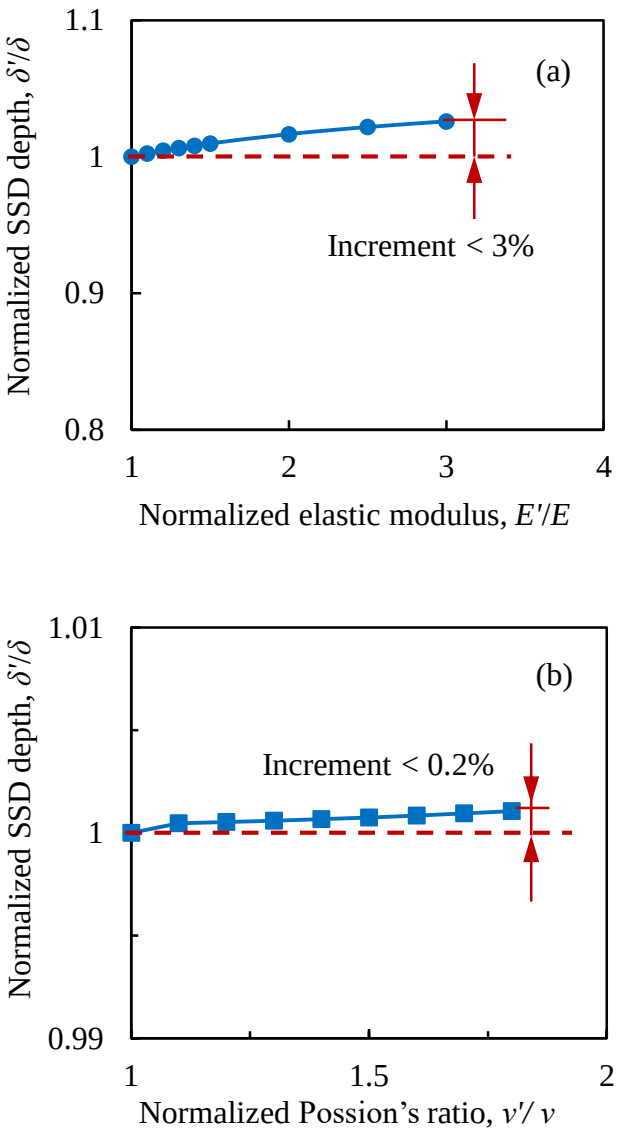

Fig. 10: Variations of SSD depth with (a) elastic modulus and (b) Poisson's ratio

5. Discussion

This paper focuses on the depth of crack formation in the silicon wafers subjected to the self-rotating grinding process. Although fracture mechanics has been applied to studying SSD formation in silicon wafers, it does not consider dislocation kinetics. Fracture mechanics is generally used to handle problems with large cracks. However, in a grinding process, cracks induced by the process are typically small simply because DOC for abrasive grains is in the range of tens of nanometers [4, 6]. Under such a condition, the effects of dislocation kinetics on SSD formation could be compared to that of the brittle fracture. Based on the TEM result, as shown in Fig. 5 (b), dislocation clusters are observed beneath a ground surface of the silicon wafer, which demonstrates plastic deformation accompanying the brittle fracture during grinding. Therefore, it is reasonable to consider not only brittle fracture but also plastic deformation in the

evolution of SSD.

Plastic deformation is dependent on dislocation motion which is driven by strain rate. Dislocation speed increases with strain rate. However, in a material, dislocation speed cannot be increased without a limit. It is generally lower than the sound speed. The behavior of dislocations may include multiplication, entanglement, annihilation, and immobilization. At a high strain rate, dislocation speed approaches to the sound speed. In this situation, the dislocation motion cannot accommodate the load applied, more new dislocations are generated and run at a speed approaching to the sound speed, which may result in the dislocation avalanche [34].

During the motion of dislocations, dislocations tend to kink, entangle each other, and form L-C locks because of their mutual interactions. L-C locks, in turn, obstruct the further dislocation motion and result in the dislocation immobilization. If the locks and junctions cannot be unzipped by the stress applied to the mobile dislocations connected to them, the locks and junctions zip further [28], which leads to stress concentration and even crack initiation if the stress exceeds the strength of a material. The destruction of the locks involves higher stress. If the dislocations around the locks cannot accommodate the destruction energy of the locks, cracks should occur.

Ahead of a crack tip, dislocations are usually distributed. The dislocations nearby a crack tip are attracted to the crack tip by the free surface image force, which forms a dislocation-free region at the crack tip. The far surround dislocations shield the crack tip and reduce the applied stress intensity factor at the crack tip [56]. The stress singularity at a crack tip is reduced by the dislocations around the crack tip because of the dislocation shielding, i.e., the plastic deformation at the crack tip is suppressed. Correspondingly, the crack tip propagates to initiate brittle fracture, which satisfies the Griffith fracture criteria that do not normally consider the contribution of dislocations to the crack nucleation.

There is a gap between the theories of dislocation kinetics and fracture mechanics. The theory of dislocation kinetics deals with dislocation nucleation, interactions, immobilization, and finally crack initiation, but without consideration of crack propagation. The fracture mechanics derives from the Griffith assumption, i.e., crack propagating from a pre-existing flaw, but without any consideration of the initiation of the flaw [13]. This paper fills the gap between the two theories by considering that the plastic deformation and brittle fracture are the two sequential stages of a crack formation. The plastic deformation breeds the brittle fracture and the formation of SSD. The two theories can be applied to the corresponding stages. Therefore, this paper integrates the theory of dislocation kinetics and the theory of fracture mechanics to link crack initiation and propagation in sequence and build a more realistic SSD depth model. The integration of the two independent theories should also be applicable to other brittle material, such as SiC, GaN, and diamond.

Given the anisotropy of monocrystalline silicon, many studies have tried to model and predict SSD depth along different crystal directions. Generally, they predicted SSD depth in a specific crystal plane individually based on the mechanical properties of the crystal plane, ignoring the influence of the different crystal planes during the propagation process of a crack [5]. Although Zhang et al. [4] considered the contributions of other crystal planes to the damage depth along one crystal direction, they hardly provided the details on how much the contributions were from other crystal planes. Due to the complicated stress distribution during the crack propagation process, the influence of the related crystal planes on the damage depth remains unclear. Besides, the difference in the measured damage depth is caused by the observation direction. The depth of the same subsurface crack is different when it is observed and measured from different crystal orientations [52]. Therefore, it is difficult to ingeniously and precisely consider the influence of all crystal planes in modelling. This paper averages the influence of different crystal planes by using the average properties to build the model, which is somewhat simple but reasonable.

Based on the proposed model, a grinding process can be divided into three stages, as indicated in Fig. 11, they are cut-in stage, fast grinding stage, and wheel lifting stage, respectively. The parameters used in the three different stages are different. In the cut-in stage, the feed rate should be large to reduce the time of cut-in as much as possible. Entering the fast grinding stage, wheel speed should be rapidly elevated to a high level to achieve a high strain rate, so as to enhance the material dynamic brittleness and thus to suppress the depth of damage. Meanwhile, the feed rate should be held at a high level to achieve a high material removal rate. Since the grain DOC is the dominant factor in the depth of damage when entering the wheel lifting stage, feed rate should be kept low, based on Eq. (21), the grain DOC is thereby reduced. In the wheel lifting stage, grinding temperature maybe high, which may cause workpiece burn [53], the wheel speed is set to decrease correspondingly with the feed rate to reduce frictional heat as well as to facilitate cooling. During this stage, the strain rate still remains at a high level. The reason is to maintain the material dynamic brittleness and thus to suppress the heat production by plastic deformation and the depth of damage as much as possible. After the grinding process finishes, the depth of damage can be minimized. By this strategy, higher grinding efficiency and high surface quality of silicon wafers can be realized. Moreover, the strategy should also be applicable to machining other brittle materials.

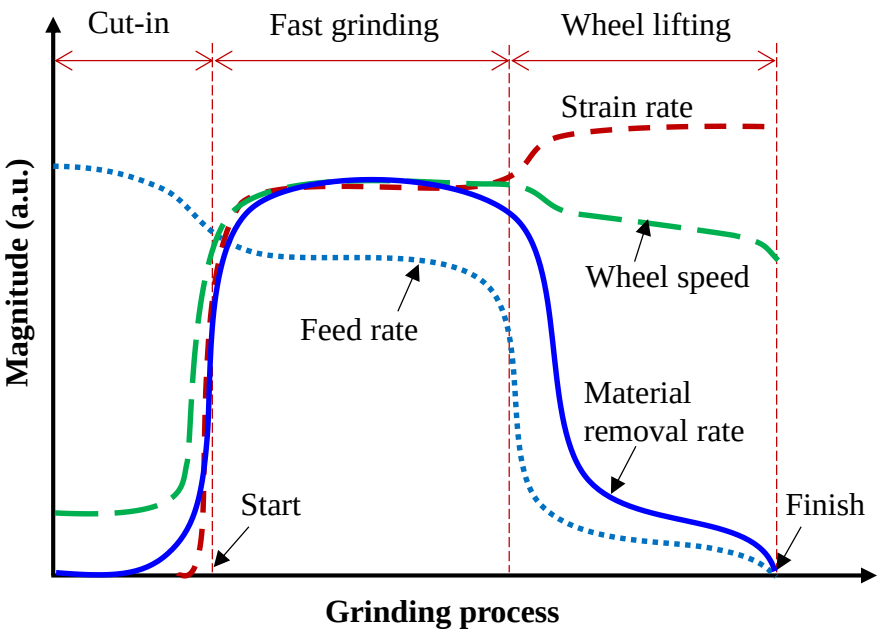

Fig. 11: Material removal rate in the whole grinding process of silicon wafer.

6. Conclusion

The paper proposes a physical model for predicting sub-surface damage (SSD) depth in monocrystalline silicon wafers subjected to self-rotating grinding. The model integrates the theory of dislocation kinetics for crack initiation with the theory of fracture mechanics for crack propagation for the first time. It considers the effects of strain rate on material property change and SSD depth in grinding. The model provides a good prediction of SSD depth, which is verified by the experimental results. Increasing strain rate enhances the material dynamic brittleness and suppresses the SSD depth. The study demonstrates a pathway to further optimizing the nanoscale grinding process and to achieve improved surface integrity during machining of silicon wafers, which is a current micromanufacturing challenge.

Acknowledgements

Financial supports from the National Natural Science Foundation of China (Grants No. 51575084 and 51605077), the Peacock Program of Shenzhen (KQJSCX20180322152221965 and KQTD20190929172505711), and the Project Funded by China Postdoctoral Science Foundation (No. 2020TQ0149) are gratefully acknowledged.

The cross-exchange became possible due to the financial support provided by the UKRI via Grants No. EP/L016567/1, EP/S013652/1, EP/S036180/1, EP/T001100/1 and EP/T024607/1, Royal Academy of Engineering via Grants No. IAPP18-19\295, TSP1332 and EXPP2021\1\277, EU Cost Actions CA15102, CA18125, CA18224 and CA16235 and Newton Fellowship award from the Royal Society NIF\R1\191571.

SG is particularly thankful to European Regional Development Funds (ERDF)

sponsored A2i project at LSBU that have catalyzed several industrial partnerships. The work used Isambard Bristol HPC service accessed by Resource Allocation Panel (RAP) grant as well as ARCHER resources (Project e648).

Reference:

[1] S. Goel, X. Luo, A. Agrawal, R.L. Reuben, Diamond machining of silicon: A review of advances in molecular dynamics simulation, International Journal of Machine Tools and Manufacture, 88 (2015) 131-164.https://doi.org/10.1016/j.ijmachtools.2014.09.013

[2] X. Luo, S. Goel, R.L. Reuben, A quantitative assessment of nanometric machinability of major polytypes of single crystal silicon carbide, Journal of the European Ceramic Society, 32 (2012) 3423-3434.https://doi.org/10.1016/j.jeurceramsoc.2012.04.016

[3] L. Wang, Y. Gao, X. Li, T. Pu, Y. Yin, Analytical prediction of subsurface microcrack damage depth in diamond wire sawing silicon crystal, Materials Science in Semiconductor Processing, 112 (2020) 105015.https://doi.org/10.1016/j.mssp.2020.105015

[4] L. Zhang, P. Chen, T. An, Y. Dai, F. Qin, Analytical prediction for depth of subsurface damage in silicon wafer due to self-rotating grinding process, Current Applied Physics, 19 (2019) 570-581.https://doi.org/10.1016/j.cap.2019.02.015

[5] H.N. Li, T.B. Yu, L.D. Zhu, W.S. Wang, Analytical modeling of grinding-induced subsurface damage in monocrystalline silicon, Materials & Design, 130 (2017) 250-262.https://doi.org/10.1016/j.matdes.2017.05.068

[6] J. Sun, F. Qin, P. Chen, T. An, A predictive model of grinding force in silicon wafer self-rotating grinding, International Journal of Machine Tools and Manufacture, 109 (2016) 74-86.https://doi.org/10.1016/j.ijmachtools.2016.07.009

[7] B. Lawn, R. Wilshaw, Indentation fracture: principles and applications, Journal of Materials Science, 10 (1975) 1049-1081. https://doi.org/10.1007/BF00823224

[8] W. Gu, Z. Yao, K. Li, Evaluation of subsurface crack depth during scratch test for optical glass BK7, Proceedings of the Institution of Mechanical Engineers, Part C: Journal of Mechanical Engineering Science, 225 (2011) 2767-2774. https://doi.org/10.1177/0954406211412458

[9] C. Li, F. Zhang, B. Meng, L. Liu, X. Rao, Material removal mechanism and grinding force modelling of ultrasonic vibration assisted grinding for SiC ceramics, Ceramics International, 43 (2017) 2981-2993.https://doi.org/10.1016/j.ceramint.2016.11.066

[10] Y. Wang, B. Lin, S. Wang, X. Cao, Study on the system matching of ultrasonic vibration assisted grinding for hard and brittle materials processing, International Journal of Machine Tools and Manufacture, 77 (2014) 66-73.https://doi.org/10.1016/j.ijmachtools.2013.11.003

[11] S. Malkin, T.W. Hwang, Grinding Mechanisms for Ceramics, CIRP Annals, 45 (1996) 569-580.https://doi.org/10.1016/S0007-8506(07)60511-3

[12] B. Zhang, T.D. Howes, Subsurface Evaluation of Ground Ceramics, CIRP Annals, 44 (1995) 263-266.https://doi.org/10.1016/S0007-8506(07)62322-1

[13] A.A. Griffith, VI. The phenomena of rupture and flow in solids, Philosophical Transactions of the Royal Society of London. Series A, Containing Papers of a Mathematical or Physical Character, 221 (1921) 163-198.https://doi.org/10.1098/rsta.1921.0006

[14] Y. Gao, P. Ge, T. Liu, Experiment study on electroplated diamond wire saw slicing single-crystal silicon, Materials Science in Semiconductor Processing, 56 (2016) 106-

114.https://doi.org/10.1016/j.mssp.2016.08.003
[15] T. Liu, P. Ge, W. Bi, Y. Gao, Subsurface crack damage in silicon wafers induced by resin bonded diamond wire sawing, Materials Science in Semiconductor Processing, 57 (2017) 147-156.https://doi.org/10.1016/j.mssp.2016.10.021
[16] C. Wang, Q. Fang, J. Chen, Y. Liu, T. Jin, Subsurface damage in high-speed grinding of brittle materials considering kinematic characteristics of the grinding process, The International Journal of Advanced Manufacturing Technology, 83 (2016) 937-948.https://doi.org/10.1007/s00170-015-7627-8
[17] L. Wan, Z. Liu, Z. Deng, L. Li, W. Liu, Simulation and experimental research on subsurface damage of silicon nitride grinding, Ceramics International, 44 (2018) 8290-8296.https://doi.org/10.1016/j.ceramint.2018.02.014
[18] W. Liu, Z. Deng, Y. Shang, L. Wan, Effects of grinding parameters on surface quality in silicon nitride grinding, Ceramics International, 43 (2017) 1571-1577.https://doi.org/10.1016/j.ceramint.2016.10.135
[19] Y. Li, N. Zheng, H. Li, J. Hou, X. Lei, X. Chen, Z. Yuan, Z. Guo, J. Wang, Y. Guo, Q. Xu, Morphology and distribution of subsurface damage in optical fused silica parts: Bound-abrasive grinding, Applied Surface Science, 257 (2011) 2066-2073.https://doi.org/10.1016/j.apsusc.2010.09.051
[20] Y. Liu, B. Li, C. Wu, Y. Zheng, Simulation-based evaluation of surface micro-cracks and fracture toughness in high-speed grinding of silicon carbide ceramics, The International Journal of Advanced Manufacturing Technology, 86 (2016) 799-808.https://doi.org/10.1007/s00170-015-8218-4
[21] C. Wu, B. Li, Y. Liu, J. Pang, S.Y. Liang, Strain rate-sensitive analysis for grinding damage of brittle materials, The International Journal of Advanced Manufacturing Technology, 89 (2017) 2221-2229. https://doi.org/10.1007/s00170-016-9237-5
[22] S. Goel, I. Llavori, A. Zabala, C. Giusca, S.C. Veldhuis, J.L. Endrino, The possibility of performing FEA analysis of a contact loading process fed by the MD simulation data, International Journal of Machine Tools and Manufacture, 134 (2018) 79-80.https://doi.org/10.1016/j.ijmachtools.2018.07.003
[23] J. Yan, H. Takahashi, J.i. Tamaki, X. Gai, H. Harada, J. Patten, Nanoindentation tests on diamond-machined silicon wafers, Applied Physics Letters, 86 (2005) 181913. https://doi.org/10.1063/1.1924895
[24] R. Limbach, B.P. Rodrigues, L. Wondraczek, Strain-rate sensitivity of glasses, Journal of Non-Crystalline Solids, 404 (2014) 124-134.https://doi.org/10.1016/j.jnoncrysol.2014.08.023
[25] M.M. Chaudhri, J.K. Wells, A. Stephens, Dynamic hardness, deformation and fracture of simple ionic crystals at very high rates of strain, Philosophical Magazine: A Journal of Theoretical Experimental and Applied Physics, 43 (1981) 643-664.https://doi.org/10.1080/01418618108240400
[26] R.J. Stokes, T.L. Johnston, C.H. Li, Crack formation in magnesium oxide single crystals, The Philosophical Magazine: A Journal of Theoretical Experimental and Applied Physics, 3 (1958) 718-725. https://doi.org/10.1080/14786435808237008
[27] F. Ebrahimi, L. Kalwani, Fracture anisotropy in silicon single crystal, Materials Science and Engineering: A, 268 (1999) 116-126.https://doi.org/10.1016/S0921-5093(99)00077-5
[28] V. Bulatov, F.F. Abraham, L. Kubin, B. Devincre, S. Yip, Connecting atomistic and mesoscale simulations of crystal plasticity, Nature, 391 (1998) 669-672.https://doi.org/10.1038/35577
[29] S.Z. Chavoshi, S. Xu, X. Luo, Dislocation-mediated plasticity in silicon during nanometric cutting: A molecular dynamics simulation study, Materials Science in Semiconductor Processing, 51 (2016) 60-70.https://doi.org/10.1016/j.mssp.2016.05.003
[30] S.Z. Chavoshi, X. Luo, Molecular dynamics simulation study of deformation mechanisms in 3C–SiC during nanometric cutting at elevated temperatures, Materials Science and Engineering: A, 654

(2016) 400-417.https://doi.org/10.1016/j.msea.2015.11.100
[31] A.M. Kovalchenko, Y.V. Milman, On the cracks self-healing mechanism at ductile mode cutting of silicon, Tribology International, 80 (2014) 166-171.https://doi.org/10.1016/j.triboint.2014.07.003
[32] S. Goel, A. Kovalchenko, A. Stukowski, G. Cross, Influence of microstructure on the cutting behaviour of silicon, Acta Materialia, 105 (2016) 464-478. https://doi.org/10.1016/j.actamat.2015.11.046
[33] S. Shim, H. Bei, E.P. George, G.M. Pharr, A different type of indentation size effect, Scripta Materialia, 59 (2008) 1095-1098.https://doi.org/10.1016/j.scriptamat.2008.07.026
[34] B. Zhang, J. Yin, The 'skin effect' of subsurface damage distribution in materials subjected to high-speed machining, International Journal of Extreme Manufacturing, 1 (2019) 012007. https://doi.org/10.1088/2631-7990/ab103b
[35] D. Tabor, The hardness of solids, Reviews of Physics in Technology, 1 (1970) 145-179. https://doi.org/10.1088/0034-6683/1/3/i01
[36] L. Kogut, K. Komvopoulos, Analysis of the spherical indentation cycle for elastic–perfectly plastic solids, Journal of Materials Research, 19 (2004) 3641-3653. https://doi.org/10.1557/JMR.2004.0468
[37] Z. Song, K. Komvopoulos, Elastic–plastic spherical indentation: Deformation regimes, evolution of plasticity, and hardening effect, Mechanics of Materials, 61 (2013) 91-100.https://doi.org/10.1016/j.mechmat.2013.01.003
[38] F. Yang, I. Kao, Free abrasive machining in slicing brittle materials with wiresaw, Journal of Electronic Packaging, 123 (2001) 254-259. https://doi.org/10.1115/1.1348019
[39] G.M. Pharr, D.S. Harding, W.C. Oliver, Measurement of Fracture Toughness in Thin Films and Small Volumes Using Nanoindentation Methods, in: M. Nastasi, D.M. Parkin, H. Gleiter (Eds.) Mechanical Properties and Deformation Behavior of Materials Having Ultra-Fine Microstructures, Springer Netherlands, Dordrecht, 1993, pp. 449-461. https://doi.org/10.1007/978-94-011-1765-4_29
[40] Y. Mai, B.R. Lawn, Crack stability and toughness characteristics in brittle materials, Annual Review of Materials Science, 16 (1986) 415-439. https://doi.org/10.1146/annurev.ms.16.080186.002215
[41] G.L. Pearson, W.T. Read, W.L. Feldmann, Deformation and fracture of small silicon crystals, Acta Metallurgica, 5 (1957) 181-191.https://doi.org/10.1016/0001-6160(57)90164-5
[42] G. Regazzoni, U.F. Kocks, P.S. Follansbee, Dislocation kinetics at high strain rates, Acta Metallurgica, 35 (1987) 2865-2875.https://doi.org/10.1016/0001-6160(87)90285-9
[43] U.F. Kocks, A.S. Argon, M.F. Ashby, Thermodynamics and kinetics of slip, Progress in materials science, 19 (1975) 1-281. https://doi.org/10.1016/0079-6425(75)90005-5
[44] E. Orowan, Problems of Plastic Gliding, Proceedings of the Physical Society, 52 (1940) 8. https://doi.org/10.1088/0959-5309/52/1/303
[45] E.B. Zaretsky, G.I. Kanel, Effect of temperature, strain, and strain rate on the flow stress of aluminum under shock-wave compression, Journal of Applied Physics, 112 (2012) 073504. https://doi.org/10.1063/1.4755792
[46] B.A. Remington, P. Allen, E.M. Bringa, J. Hawreliak, D. Ho, K.T. Lorenz, H. Lorenzana, J.M. McNaney, M.A. Meyers, S.W. Pollaine, K. Rosolankova, B. Sadik, M.S. Schneider, D. Swift, J. Wark, B. Yaakobi, Material dynamics under extreme conditions of pressure and strain rate, Materials Science and Technology, 22 (2006) 474-488. https://doi.org/10.1179/174328406X91069
[47] F.J. Zerilli, R.W. Armstrong, Description of tantalum deformation behavior by dislocation mechanics based constitutive relations, Journal of Applied Physics, 68 (1990) 1580-1591.10.1063/1.346636
[48] J.W. Swegle, D.E. Grady, Shock viscosity and the prediction of shock wave rise times, Journal of

Applied Physics, 58 (1985) 692-701. https://doi.org/10.1063/1.336184
[49] M.E. Kipp, D.E. Grady, E.P. Chen, Strain-rate dependent fracture initiation, International Journal of Fracture, 16 (1980) 471-478. https://doi.org/10.1007/bf00016585
[50] B. Wang, Z. Liu, G. Su, Q. Song, X. Ai, Investigations of critical cutting speed and ductile-to-brittle transition mechanism for workpiece material in ultra-high speed machining, International Journal of Mechanical Sciences, 104 (2015) 44-59.https://doi.org/10.1016/j.ijmecsci.2015.10.004
[51] R.F. Smith, R.W. Minich, R.E. Rudd, J.H. Eggert, C.A. Bolme, S.L. Brygoo, A.M. Jones, G.W. Collins, Orientation and rate dependence in high strain-rate compression of single-crystal silicon, Physical Review B, 86 (2012) 245204. https://doi.org/10.1103/PhysRevB.86.245204
[52] J. Yin, Q. Bai, Y. Li, B. Zhang, Formation of subsurface cracks in silicon wafers by grinding, Nanotechnology and Precision Engineering, 1 (2018) 172-179.https://doi.org/10.1016/j.npe.2018.09.003
[53] Z. Zhang, Y. Huo, D. Guo, A model for nanogrinding based on direct evidence of ground chips of silicon wafers, Science China Technological Sciences, 56 (2013) 2099-2108. https://doi.org/10.1007/s11431-013-5286-2
[54] D. Hayes, R.S. Hixson, R.G. McQueen, High pressure elastic properties, solid-liquid phase boundary and liquid equation of state from release wave measurements in shock-loaded copper, AIP Conference Proceedings, 505 (2000) 483-488. https://doi.org/10.1063/1.1303521
[55] J. Zhou, J. Liu, X. Zhang, Y. Yan, L. Jiang, I. Mohagheghian, J.P. Dear, M.N. Charalambides, Experimental and numerical investigation of high velocity soft impact loading on aircraft materials, Aerospace Science and Technology, 90 (2019) 44-58.https://doi.org/10.1016/j.ast.2019.04.015
[56] B.S. Majumdar, S.J. Burns, Crack tip shielding—An elastic theory of dislocations and dislocation arrays near a sharp crack, Acta Metallurgica, 29 (1981) 579-588.https://doi.org/10.1016/0001-6160(81)90139-5
[57] M.M. Islam, A.S. Kumar, S. Balakumar, H.S. Lim, M. Rahman, Characterization of ELID grinding process for machining silicon wafers, Journal of Materials Processing Technology, 198 (2008) 281-290.https://doi.org/10.1016/j.jmatprotec.2007.06.077
[58] J. Li, Q. Fang, L. Zhang, Y. Liu, Subsurface damage mechanism of high speed grinding process in single crystal silicon revealed by atomistic simulations, Applied Surface Science, 324 (2015) 464-474.https://doi.org/10.1016/j.apsusc.2014.10.149